PRACE INSTYTUTU ODLEWNICTWA
TRANSACTIONS OF FOUNDRY RESEARCH INSTITUTE

Volume LVII Year 2017 Number 4

Thermophysical properties of selected vermicular graphite cast iron alloy

Marta Homa[1], Natalia Sobczak[1,2], Patrycja Turalska[1], Grzegorz Bruzda[1], Magdalena Bacior[3], Małgorzata Warmuzek[1], Adelajda Polkowska[1]

[1]Foundry Research Institute, ul. Zakopiańska 73, 30-418 Krakow, Poland
[2]Institute of Precision Mechanics, ul. Duchnicka 3, 01-796 Warsaw, Poland
[3]University of Agriculture in Krakow, Department of Physics, al. A. Mickiewicza 21, 31-120 Krakow, Poland

E-mail: marta.homa@iod.krakow.pl

Received: 06.11.2017. Accepted in revised form: 29.12.2017.

DOI: 10.7356/iod.2017.36

Abstract

The paper presents the results of thermophysical properties of selected vermicular graphite cast iron with nominal chemical composition of 3.70 C; 2.30 Si; 0.44 Mn; 0.054 P; 0.015 S; 0.017 Mg (wt. %). The comparative studies of the alloy were performed using differential scanning calorimetry, dilatometry and laser flash analysis. The calorimetric investigations proved that upon the heating to melting temperature (~1200°C), four endothermic transformations take place: 1) ferromagnetic → paramagnetic at 742°C, 2) pearlite → austenite at 824.2°C, 3) allotropic transformation of bcc ferrite to fcc austenite at 802°C, 4) melting at 1173.1°C. The character of the dilatometric curve shows small deviation at the temperature above 810°C corresponding to the pearlite → austenite transformation. The values of thermal diffusivity and thermal conductivity change throughout the entire examined temperature range. Both curves showed a changeover from negative to positive trends between 700 and 800°C. This effect might be associated with the pearlite → austenite transformation.

Keywords: *vermicular cast iron, thermophysical properties, transformation temperatures, melting heat, thermal expansion, thermal expansion coefficient, thermal diffusivity, thermal conductivity*

1. Introduction

The vermicular graphite cast iron (VG iron) has already been widely used as an engineering alloy [1]. This material is a part of cast iron family belonging to Fe-C irregular eutectic system characterized by an intermediate graphite morphology placed between flake and nodular graphite cast irons (FG and NG, respectively) [2].

With respect to its structure and/or physico-mechanical properties, the VG iron is a grade between FG and NG cast iron [3].

Compared to NG, the VG iron has a comparable coefficient of thermal expansion but higher thermal conductivity, better castability and lower tendency for contraction cavity formation, as well as a higher thermal fatigue resistance. Compared to FG iron, the VG iron has higher resistance to oxidation at elevated temperatures ductility and higher modulus of elasticity [2,4,5]. Due to these advantages, the VG iron finds a wide range of specific applications i.e. for the cylinder heads of high power density diesel engines [6].

The research procedure, measurement methods as well as theoretical and experimental data on solid state thermophysical properties of selected vermicular cast iron are showed in this work. The material is a reference to studies carried out in connection with implementation of project entitled: “High temperature investigations of the effect of alloying on thermophysical properties of liquid cast iron and its wettability and reactivity in contact with metal oxides”. These results will be discussed in details in the next publication devoted to comparative studies on influence of alloying additions i.e. Mo, Cu, V, Sn and Sb on thermophysical properties of selected cast irons.

2. Testing methodology

2.1. Materials

The selected VG iron was melted using charge composed with pig iron, steel scrap, ferromanganese and ferrosilicon. Such composition of alloy was chosen to make the base cast iron having a chemical composition

Table 1. The chemical composition of charge, magnesium master alloy, inoculant and alloy as-cast state

Sample	Chemical composition, wt. %										
	Fe	C	Si	Mn	P	S	Mg	Al	Ca	Ba	RE
S1	–	–	44.0−48.0	–	–	–	5.6−6.0	max. 1.0	1.8−2.3	–	5.5−6.5
S2	–	–	73.0−78.0	–	–	–	–	0.75−1.25	0.75−1.25	0.75−1.25	–
S3	Bal.	3.7	2.3	0.44	0.054	0.015	0.017	max.1.0	–	–	–

corresponding to hypereutectic cast iron with saturation coefficient higher than 1.0. All preparation procedure was performed in Foundry Research Institute according to the following 3 steps:

– the 1st step – a melting process with using an induction Radyne furnace with inert crucible lining [7];

– the 2nd step – a vermiculitizing process at temperature range of 1440−1450°C with magnesium containing (Mg <6%) master alloy (S1);

– the 3rd step – a inoculation process with inoculant (S2).

The chemical composition of charge, magnesium master alloy, the inoculant, alloy as-cast state are presented in Table 1. The contents of the elements in as-cast state were determined by spectrometry analysis (S3).

The ingot was cast and then samples for observations of structure, calorimetric, dilatometric and thermal properties studies, were cut. The structural observations of the sample in the as-cast state and after calorimetric test were carried out using Zeiss Observer.21m optical microscope (OM) (by using the magnifications up to 500×).

2.2. Research procedure

The measurements of thermophysical properties were carried out according to the procedure developed in the Foundry Research Institute (Fig. 1).

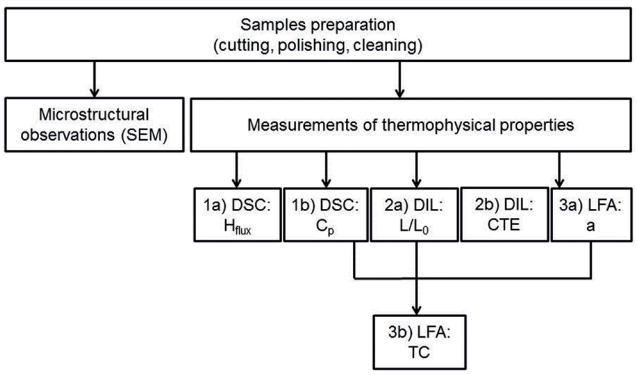

Fig. 1. A scheme showing research procedure

In order to characterize the thermophysical properties, the following measurement techniques were used:

1. Differential scanning calorimetry (DSC). The measurements were performed by means of the Netzsch DSC 404 C/3/G Pegasus differential scanning calorimeter in order to evaluate:

   1a) heat flux (H_{flux});
   1b) specific heat (C_p).

2. Dilatometry (DIL). The measurements were conducted with the use of Netzsch DIL 402C/4/G high-temperature dilatometer in order to evaluate:

   2a) thermal expansion (L/L_0);
   2b) coefficient of thermal expansion (CTE).

3. Laser flash analysis (LFA). The measurements were performed with the application of the Netzsch LFA 427 apparatus.

   3a) coefficient of temperature diffusivity (a);
   3b) thermal conductivity (TC).

Thermal conductivity was determined with the consideration of the radiation losses based on the non-linear regression, the Cape-Lehman model [8] and equation:

$$TC(T) = a(T)\, c_p(T)\, \frac{L}{L_0}(T) \qquad (1)$$

where:

$TC(T)$ – thermal conductivity vs. temperature,

$a(T)$ – thermal diffusivity vs. temperature,

$L/L_0\ (T)$ – thermal expansion vs. temperature.

The measurement accuracy of the LFA technique, by taking into account errors in the determination of other thermophysical values, is not inferior to the accuracy of the so-called “direct” methods of the estimation of TC, based on calculations of this parameter from the results of heat flux measurements (through temperature gradients) and measurements of the sample geometric parameters assuming steady state conditions [9].

Table 2. Experimental conditions used upon examinations of thermophysical properties

Measurement technique	Conditions					
	Sample size, mm	Temperature, °C	Pressure, Pa	Atmosphere	Gas flow, ml/min	Heating/cooling rate, K/min
DSC: H_{fulx}	≤ 200 mg	25−1200	–	Ar	70	10
DSC: C_p		25−1000				5
DIL	2 × 2 × 10 mm	25−1000				5
LFA	10 × 10 × 2 mm	25−1000	1×10^{-2}	Vacuum	–	10

2.3. Preparation of samples and testing conditions

Specimens were cut off from the as-cast ingot in order to meet dimensions of sample holders in used apparatus. The dimensions of sample holders are listed in Table 2. Before experiments, samples were degreased in isopropanol and dried in air. In the case of LFA measurements, the front surfaces of the sample was covered with a graphite spray to supress the effect of radiation. All experimental conditions are collected in Table 2.

3. Results and discussion

Microstructure of the cast iron was examined on the metallographic cross sections, observed by means of light microscope. The graphite morphology and distribution, were identified based on PN-EN ISO 945-1 standard [10] while the structure of matrix – based on PN-75/H-04661archival standard [11]. The materials in its as-cast state was characterized by ferritic-pearlitic structure (estimated fraction of ferrite was about 70−90%). The 98% of graphite precipitates have had a vermicular morphology, while the rest of them was spheroidal (Fig. 2a,b). Furthermore, fine areas of phosphide eutectic were also observed inside pearlite zones on grain boundaries (Fig. 2b).

After the C_p test an increase of the volume fraction of the perlite, was observed. The volume fraction of ferrite was estimated as 20% (Fig. 3). One can state that during annealing in solid state almost complete austenitization of the matrix takes place and, in consequence, perlite is formed through eutectoid transformation austenite → ferrite + Fe_3C when the specimen is cooled down.

The microscopic characterization of the specimen that was melted and then slowly cooled down (10 K/min) to room temperature upon the DSC test, revealed prominent structural changes (Fig. 4). Vermicular precipitates of graphite did not re-grow after the solidification. Graphite precipitates took shape of flakes having a different dispersion degree. The graphite rosettes reflecting eutectic cells morphology were formed in the examined specimen. Perlite was the main microstructure constituent as a result of the eutectoid transformation: austenite → ferrite + Fe_3C.

These results show that after the complete melting of the vermicular cast iron the reconstruction of the primary vermicular morphology of graphite, is not possible. One can assume that modifiers, determining vermicular graphite morphology stopped working. It means that growth in $[10\bar{1}0]$ direction was activated and dominated in eutectic graphite crystals [12,13]. Although, a lot of theories of vermicular graphite growth are still considered [14−16] an important role of the microsegregation of certain trace elements (modifiers) in the liquid channels

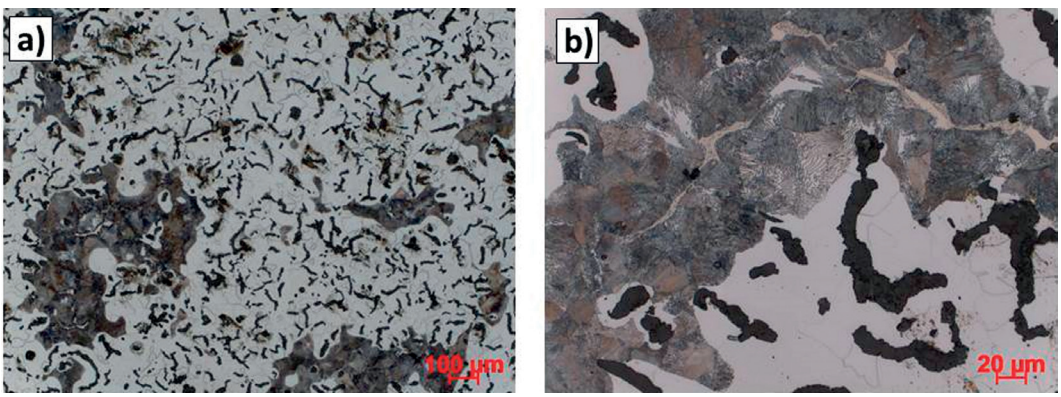

Fig. 2. Microstructure of the examined VG iron in as-cast state: a) 100×, b) 500×, LM, metallographic cross section, chemical etching with 4% Nital reagent

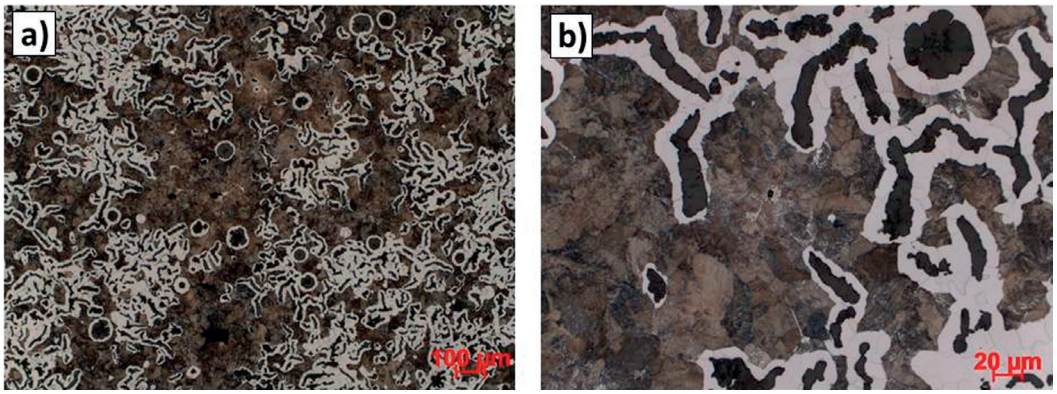

Fig. 3. The microstructure of examined VG iron after Cp test carried out at temperature up to 1000°C: a) 100×, b) 500×, LM metallographic cross section, chemical etching with 4% Nital reagent

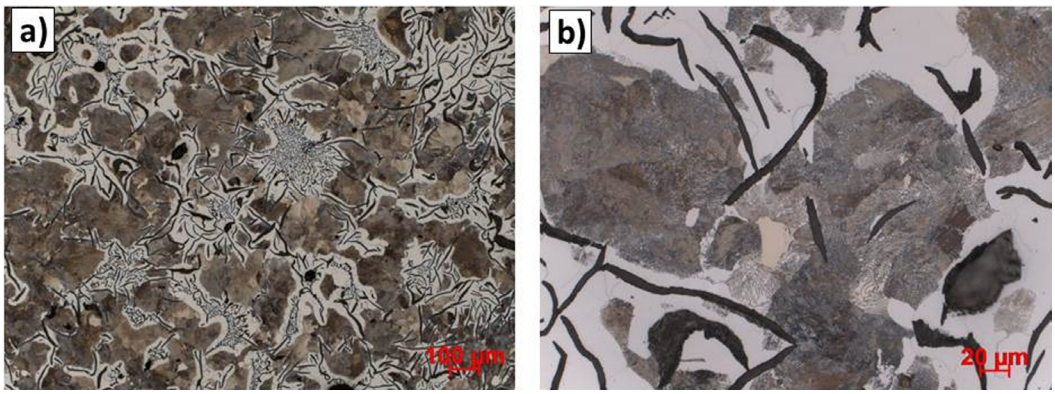

Fig. 4. The microstructure of examined VG iron after the melting and solidification during the DSC test up to 1200°C: a) 100×, b) 500×, LM metallographic cross section, chemical etching with 4% Nital reagent

in the austenite shell around the primary precipitate, is mainly accepted. Thus, the re-growth of vermicular form of graphite becomes impossible, when necessary local concentration of the modifiers in these liquid channels is destroyed during the complete melting of alloy [14,15].

The process heating and melting of VG iron has a complex character, and its mainly determined by the formation of different phases, which can successively change and transform to the another.

The calorimetric investigations revealed that during the heating to melting temperature, four endothermic transformations take place in the VG iron (Fig. 5a). The first endothermic effect has extremum at the temperature of 742°C and is related with magnetic transformation at Curie temperature [17]. It should be noted, that although the temperature Curie for pure iron is 770°C, it has been already recognized [18] that most of alloying additives lower this temperature in iron-based alloys. The second endothermic effect showing a peak maximum at temperature of 788.3°C results from the pearlite → austenite transformation. Due to a diffusion-based nature of this transformation it is within the temperature range of 775 to 800°C during the heating with the rate of 10 K/min.

The third and the most pronounced endothermic event that was started at 802°C and ended at 860.5°C is as-

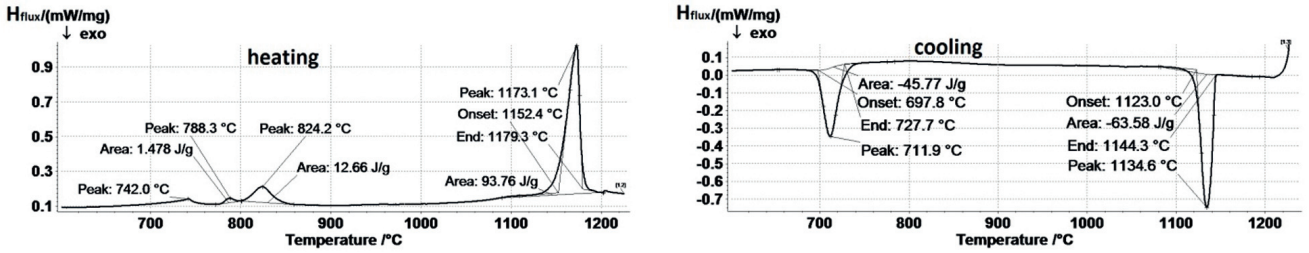

Fig. 5. The DSC curve of VG iron acquired during: a) heating to 1200°C and b) cooling at 10 K/min

sociated with the allotropic transformation of bcc ferrite to fcc austenite.

The last endothermic effect is due to the melting process. This effect starts at eutectic temperature 1152.3°C and has the extremum at a temperature of 1173.1°C. The value of transformation enthalpy (ΔH) was 93.76 J/g. The value of supercooling was 9.7°C (Fig. 5b). The heat flux results are correlated with C_p curve. The determination of specific heat curve, generally change with temperature, reaching a maximum during a phase transformation occurs (Fig. 6).

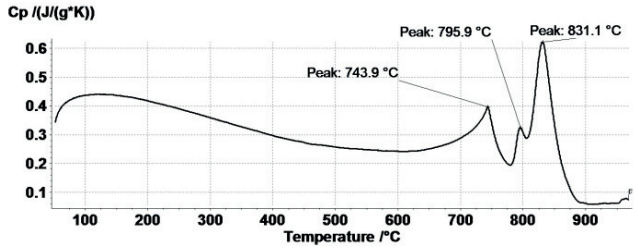

Fig. 6. The C_p curve as a function of temperature

Table 3 gives the characteristic transformation temperatures with the corresponding values of enthalpy.

Table 3. Characteristic transformation temperatures

Transformation	Temperature, °C			Enthalpy, J/g
	Onset	Maximum	End	
magnetic	–	742.0	–	–
pearlite → austenite	775.0	788.3	800.0	1.5
bcc ferrite → fcc austenite	802.0	824.2	860.5	12.7
melting	1152.4	1173.1	1179.3	93.6

The dilatometric results (Fig. 7) indicate that with rising temperature in the entire examined range, the relative dimensional changes are at a similar level. At a temperature range of 810−830°C, the curves show a deviation corresponding to the pearlite → austenite transformation. The value of final increment was 0.00168.

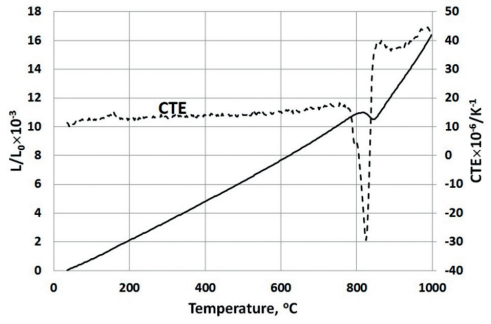

Fig. 7. Change of thermal expansion (L/L_0) and coefficient of thermal expansion (CTE) vs. temperature

Changes in thermal diffusivity and thermal conductivity calculated from the experimental data of ($L/L_0(T)$, $C_p(T)$ and $a(T)$) are compared in Figure 8.

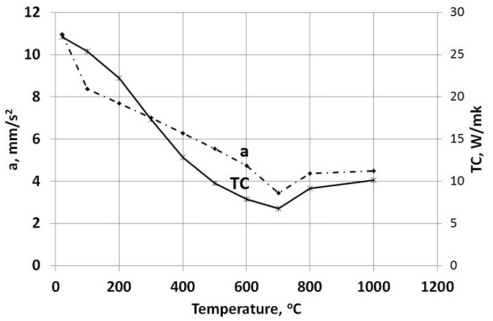

Fig. 8. Thermal diffusivity (a) and thermal conductivity (TC) vs. temperature plots

The values of a and TC change throughout the entire examined temperature range. At temperature range of 25 to 700°C the values of a and TC decrease to a = 3.45 mm · s^{-1} and TC = 6.75 $Wm^{-1} \cdot K^{-1}$. Above 700°C, these values increase and at 1000°C they are equal to a = 4.50 mm · s^{-1} and TC = 10.12 $Wm^{-1} \cdot K^{-1}$. The observed shape of the curves with a minimum at 700°C, should be associated with a presence of bcc → fcc transformation of iron crystal lattice taking place at 723°C. Nevertheless, a greater amount of measurement points is needed to confirm this finding.

4. Conclusions

Based on the results of structural examinations carried out by means of optical microscopy and examinations of thermo-physical properties performed by DSC, DIL, LFA it can be concluded that:

1. Thermal effects recorded during heating of VG iron sample up to its melting point have complex character. Three consecutive events might be distinguished on the curves: ferromagnetic to paramagnetic transformation at the Curie point, pearlite to austenite transformation and melting.

2. The analysis of thermal expansion vs. testing temperature allows identifying the presence of pearlite → austenite transformation in the examined VG iron.

3. The values of a and TC change throughout the entire examined temperature range. Both curves showed a changeover from negative to positive trends between 700 and 800°C. This effect might be associated with the ferrite → pearlite transformation.

Acknowledgements

The research were carried out with thanks to the financial support of the National Science Centre of Poland (program OPUS, project No. 2015/17/B/ST8/03391 entitled “High temperature investigations of the effect of alloying on thermophysical properties of liquid cast iron and its wettability and reactivity in contact with metal oxides”).

References

1. Guzik E., D. Kopyciński, T. Kleingartner, M. Sokolnicki. 2012. „The structure and mechanical properties of pearlitic-ferritic vermicular cast iron”. *Archives of Foundry Engineering* 12 (1) : 33−36.

2. Gregorutti R.W., J.E. Grau. 2014. “Mechanical properties of compacted graphite cast iron with different microstructures”. *International Journal of Cast Metals Research* 27 (5) : 275−281. DOI: 10.1179/1743133614Y.0000000118.

3. Imasogie B.I. 2003. “Microstructural features and mechanical properties of compacted graphite iron treated with calcium-magnesium based masteralloy”. *Journal of Materials Engineering and Performance* 12 (3) : 239−243.

4. Guzik E., S. Dzik. 2009. “Structure and mechanical properties of vermicular cast iron in cylinder head casting”. *Archives of Foundry Engineering* 9 (1) : 175−180.

5. Gumienny G., N. Dondzbach, B. Kacprzyk. 2015. “Effect of chromium on the solidification process and microstructure of vermicular graphite cast iron”. *Archives of Foundry Engineering* 15 (3) : 29−34.

6. Ma Z.J., D. Tao, Z. Yang, Y.C. Guo, J.P. Li, M.X. Liang, L.T.L. Yeung. 2016. “The effect of vermicularity on the thermal conductivity of vermicular graphite cast iron”. *Materials and Design* 93 (March 2016) : 418−422. DOI: 10.1016/j.matdes.2015.12.169.

7. Pytel A., A. Gazda. 2014. “Evaluation of selected properties in austempered vermicular cast iron (AVCI)”. *Transactions of Foundry Research Institute* 54 (4) : 23−29. DOI: 10.7356/iod.2014.18.

8. Cape J.A., G.W. Lehman. 1963. “Temperature and finite pulse time effect in the flash method for measuring thermal conductivity”. *Journal of Applied Physics* 34 (7) : 1909−1913.

9. Gazda A., M. Homa. 2009. “Determination of thermal conductivity of selected types of ductile iron (spherodical/cast iron) by means of thermal diffusivity measurements with laser flash method”. *Transactions of Foundry Research Institute* 49 (2) : 5−18.

10. PN-EN ISO 945-1:2010. Mikrostruktura żeliwa. Cz. 1: Klasyfikacja grafitu za pomocą analizy wizualnej.

11. PN-75/H-04661. Żeliwo szare sferoidalne i ciągliwe. Badania metalograficzne. Określanie mikrostruktury (archiwalna).

12. Liu P.C., C.R. Loper, Jr., T. Kimura, H.K. Par. 1980. “Observations on the graphite morphology in cast iron”. *AFS Transactions* 88 : 97−118.

13. Qing J., V.L. Richards, D.C. Van Aken. 2017. “Growth stages and hexagonal-rhombohedral structural arrangements in spheroidal graphite observed in ductile iron”. *Carbon* 116 (May 2017) : 456−469.

14. Gan Y., C.R. Loper, Jr. 1983. “Observations on the formation of graphite in compacted and spheroidal graphite cast irons”. *AFS Transactions* 91 : 781−788.

15. Itofuji H., Y. Kawano, N. Inoyama, S. Yamamoto, B. Chang, T. Nishi. 1983. “The formation mechanism of compacted/vermicular graphite in cast irons”. *AFS Transactions* 91 : 831−840.

16. Chen J.Y., D.H. Wu, P.C. Liu, C.R. Loper, Jr. 1986. “Liquid metal channel formation in compacted/vermicular graphite cast iron solidification”. *AFS Transactions* 94 : 537−544.

17. Przeliorz R., J. Piątkowski. 2011. “Investigation of phase transformation in ductile cast iron of differential scanning calorimetry”. *IOP Conference Series: Materials Science and Engineering* 22 : 1−9. DOI: 10.88/1757-899X/22/1/012019.

18. Haglund O. 1982. “Curie temperature of alloys, its measurements and technical importance”. *Journal of Thermal Analysis* 25 (1) : 21−43.